arXiv:2304.04483v1 [hep-ph] 10 Apr 2023

Searching for Majorana Neutrinos at a Same-Sign Muon Collider

Ruobing Jiang,[a,b] **Tianyi Yang,**[a,1] **Sitian Qian,**[a] **Yong Ban,**[a] **Jingshu Li,**[c] **Zhengyun You,**[c] **Qiang Li**[a]

[a]*Department of Physics and State Key Laboratory of Nuclear Physics and Technology, Peking University, Beijing, 100871, China*

[b]*School of Physical Science and Technology, Southwest University*

[c]*School of Physics, Sun Yat-Sen University, Guangzhou 510275, China*

E-mail: tyyang99@pku.edu.cn

ABSTRACT: Majorana properties of neutrinos have long been a focus in the pursuit of possible new physics beyond the standard model, which has motivated lots of dedicated theoretical and experimental studies. A future same-sign muon collider is an ideal platform to search for Majorana neutrinos through the Lepton Number Violation process: $\mu^+\mu^+ \to W^+W^+$. Specifically, this t-channel kind of process is less kinematically suppressed and has a good advantage in probing Majorana neutrinos at high mass regions up to 10 TeV. In this paper, we perform a detailed fast Monte Carlo simulation study through examining three different final states: 1) pure-leptonic state with electrons or muons, 2) semi-leptonic state, and 3) pure-hadronic state in the resolved or merged categories. Furthermore, we perform a full simulation study on the pure-leptonic final state to validate our fast simulation results.

---

[1]Corresponding author.

Contents

1   Introduction

The discovery of the Higgs boson in 2012 [1, 2] marked a triumph of the Standard Model (SM) of particle physics and the Large Hadron Collider (LHC). The LHC and the High-Luminosity LHC (HL-LHC), together with other future colliders such as muon colliders in design, will further explore the SM and search for physics beyond that. However, despite the enormous success of SM and LHC, the observation of neutrino oscillations has confirmed that at least two SM neutrinos have small but nonzero masses, and there is flavor mixing among three-generation light neutrinos. This provides a compelling hint of physics beyond the SM, because the right-handed components of neutrinos and the tiny neutrino masses as well as the flavor mixtures of the lepton sectors are not expected in the original SM [16]. Therefore, searching for Majorana neutrinos in order to explain the origin of neutrino masses is extremely important.

Majorana neutrinos have been studied at various types of colliders, including the LHC [3–8], electron-positron collider [9–11], electron-electron collider [12], electron-proton collider [13] and muon-muon collider [14, 15]. In this paper, we focus on the inverse $0\nu\beta\beta$-like channel through same-sign muon collisions [16]: $\mu^+\mu^+ \to W^+W^+$, and perform a research on the relationship between the mass of Majorana neutrinos and the square of mixing element. The constraints on the squared mixing element between the muon and the Majorana neutrino are derived in the Majorana neutrino mass range of 100GeV– 40TeV. The results show that our signal process have unique advantages when the mass is greater than 10TeV.

2 Majorana Neutrinos and Type-I Seesaw Model

Majorana neutrinos are a common feature of many extensions of the SM, motivated by their roles in explaining the generation of neutrino masses. The simplest renormalizable extension of the SM for understanding the smallness of the left-handed neutrino masses is defined by the interaction Lagrangian :

$$- L_y = y_{\ell\alpha}\overline{L_\ell}\widetilde{\Phi} \ N_{R\alpha} + \text{H.c.} \tag{2.1}$$

where $y_{\ell\alpha}$ is the dimensionless complex Yukawa couplings, $\alpha = 1, 2, ..., N$ is the singlet neutral fermions flavor index, $\overline{L_\ell}$ corresponds to the lepton field, $\widetilde{\Phi}$ corresponds to higgs field, $N_{R\alpha}$ are singlet neutral fermions in SM. This Lagrangian generates a Dirac mass $M_D = y_{\ell\alpha}\nu$, where ν is the vacuum expectation value. Since the right-handed neutrinos carry no SM gauge charges, in order to preserve gauge invariance, we can introduce a new term of Lagrangian for Majorana mass:

$$- L_M = \frac{1}{2}(M_N)_{\alpha\beta}\overline{N}^c_{R\alpha}N_{R\beta} + \text{H.c.} \tag{2.2}$$

The two Lagrangians above together lead to the following neutrino mass matrix:

$$\begin{bmatrix} 0 & M_D \\ M_D^T & M_N \end{bmatrix} \tag{2.3}$$

So, the light neutrino masses and mixing element are given by the diagonalization of the effective mass matrix: $M_\nu \simeq M_D M_N^{-1} M_D^T$, $V_{\ell N_\alpha} \sim M_D M_N^{-1}$ [31]. Because Majorana neutrinos can only couple to the SM through mixing with SM neutrinos, so we can establish the relationship between the SM neutrinos mass and the Majorana neutrinos mass by [8]:

$$m_\nu = y_{\ell\alpha}^2 \nu^2 / m_N. \tag{2.4}$$

This is the most famous model including Majorana neutrinos: Type-I Seesaw model. This mechanism can explain neutrinos' small masses and the variations of neutrinos in SM. It directly shows that the smallness of SM neutrinos masses can be explained by a suppression due to the high mass of new particles in the Type-I seesaw mechanism.

From the above discussion, the massive Majorana neutrinos can testify the small mass of SM neutrinos and heavy Majorana neutrinos are mixed with SM neutrinos, which is characterized by the mixing element $|V_{\ell N_\alpha}|^2$, between an SM neutrino in its left-handed interaction state and a heavy Majorana neutrino in its mass eigenstate [8]. Therefore, it is clear that there are two key aspects of the Type-I seesaw mechanism that can be probed experimentally, the Majorana neutrino mass M_N, and the mixing element $|V_{\ell N_\alpha}|$. And Majorana neutrino mass will put a constraint on $|V_{\ell N_\alpha}|^2$. For the Majorana neutrinos masses above the EW boson masses, the highest sensitivity is expected for the heavy Majorana neutrino searches in the tri-lepton or same-sign di-lepton channels. Limits on the mixing elements extend down to about $10^{-5} \sim 10^{-6}$ for neutrino masses M_N at several GeV [8].
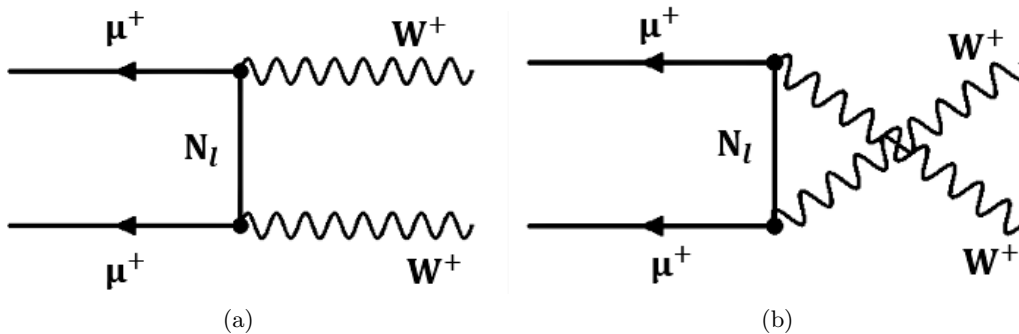
Figure 1: Signal processes at a same sign muon collider :(a) t-channel, (b) u-channel

3 Majorana Neutrinos Study at Same-Sign Muon Collider

A muon–muon collider with the center-of-mass (c.m.) energy at the multi-TeV scale has received much-revived interest [18] recently, which has several advantages compared with both hadron–hadron and electron–electron colliders [19–22]. On the one hand, as massive muons emit much less synchrotron radiation than electrons, muons can be accelerated in a circular collider to higher energies with a much smaller circumference. On the other hand, because the proton is a composite particle, muon–muon collisions are cleaner than proton–proton collisions and thus can lead to higher effective c.m. energy. However, due to the short lifetime of the muon, the beam-induced background (BIB) from muon decays needs to be examined and constrained properly. Based on a realistic simulation at $\sqrt{s} = 1.5$TeV with BIB included [23], found that the coupling between the Higgs boson and the b-quark can be measured at the percentage level with order ab^{-1} of collected data.

In this study, we perform a search of Majorana neutrinos at a same-sign muon collider. We target two benchmark scenarios in this study, i.e., a c.m. energy of 1TeV and 10TeV with a luminosity of 1 ab^{-1} , and we add a luminosity of 10 ab^{-1} for 10TeV channel to get the most sensitive result. The processes related to the mediation by Majorana neutrinos at a same-sign muon collider are shown in Fig. 1, which is sensitive to the TeV-seesaw scenario. Based on the decay channels of two W$^+$ bosons, we can divide our final states into three channels: a pure-leptonic channel with two leptons, a semi-leptonic channel with one lepton and two jets, and a pure-hadronic channel with four jets. Furthermore, we also analyze the impact of fatjets at several TeV c.m. energy.

In the following sections, we firstly discuss the kinematic properties of $\mu^+\mu^+ \rightarrow W^+W^+$ process and introduce our cut-flow strategy to reduce the background events. Then, we present our numerical analysis results and discuss the detection possibilities in all three final states. To compare the consistency of fast simulation and full simulation results, the pure-leptonic final state is studied by full simulation and compared with the fast simulation. Lastly, we give the results of limits and compare them with previous analyses.

4 Simulation and Analysis Framework

Both signal and background events are simulated with MadGraph5_aMC@NLO [40], then showered and hadronized by PYTHIA8 [27]. The final state jets are clustered using FAST-JET [28] with the k_{T} [29] algorithm at a fixed cone size of $R_{\mathrm{jet}} = 0.5$. We used DELPHES [30] version 3.0 to simulate detector effects with the default card for the muon collider detector [42]. Note that the present jet tagging techniques for muon colliders are in a preliminary stage [23] and have a large potential to be improved. In this section, we discuss in detail the three final states of the signal process introduced above: pure-leptonic state, semi-leptonic state, and hadronic state. There are seven corresponding backgrounds:

- $\mu^+\mu^+ \to \mathrm{W}^+\mathrm{W}^+\tilde{\nu}_\mu\tilde{\nu}_\mu$,

- $\mu^+\mu^+ \to \mathrm{ZW}^+\mu^+\tilde{\nu}_\mu$,

- $\mu^+\mu^+ \to \mathrm{W}^+\mu^+\nu_\mu\nu_\mu$,

- $\mu^+\mu^+ \to \mathrm{Z}\mu^+\mu^+$,

- $\mu^+\mu^+ \to \mathrm{ZZ}\mu^+\mu^+$,

- $\mu^+\mu^+ \to \mathrm{W}^+\mathrm{W}^-\mu^+\mu^+$,

- $\gamma\gamma \to \mathrm{W}^+\mathrm{W}^-$.

4.1 Pure-leptonic channel

We apply constraints on the channel $\mu^+\mu^+ \to \mathrm{W}^+\mathrm{W}^+ \to 2\ell + \not{E}_T$ at $\sqrt{s} = 1\mathrm{TeV}$ and $\mathcal{L} = 1\ \mathrm{ab}^{-1}$ are: the events must include exactly two leptons with transverse momentum $p_\mathrm{T} > 20\mathrm{GeV}$, absolute pseudo-rapidity $|\eta_\ell| < 2.5$, and $\Delta R_{\ell\ell} > 0.4$, where $\Delta R = \sqrt{(\Delta\phi)^2 + (\Delta\eta)^2}$. Fig. 2 shows some typical distributions with fast simulation, including invariant mass $M_{\ell\ell}$, transverse momentum of the leading lepton $p_{\mathrm{T},\ell\ell}$, $\cos\theta_{\ell\ell}$ ($\theta_{\ell\ell}$ is the angle between two leptons in final states) and Missing transverse energy $\not{E}_T$. Some full simulation results are also shown in Fig. 3.

In the full simulation, we generate stable input particles through standalone software, such as MadGraph5_aMC@NLO , then do parton shower through PYTHIA8. The interaction of stable particles with the detector material is simulated by GEANT4 which is closely integrated into iLCSoft framework [38] previously used in CLIC experiments, and now could be used in Muon Collider studies. Both the detector response and the event reconstruction are done within a single framework such as the modular Marlin framework [41]. The detector geometry is defined using the DD4hep detector description toolkit, which provides a consistent interface with both GEANT4 and Marlin environments [39]. We list variables distribution of signal and one background process in Fig. 3, we can find that the fast-simulation and the full-simulation give roughly similar distribution. However, due to the full-simulation can detect μ^+ in final states more accurately, there is also some difference in variables distribution between full-simulation and fast simulation, especially, the distribution of $\not{E}_T$, because there is not easy for full-simulation to contain all objects
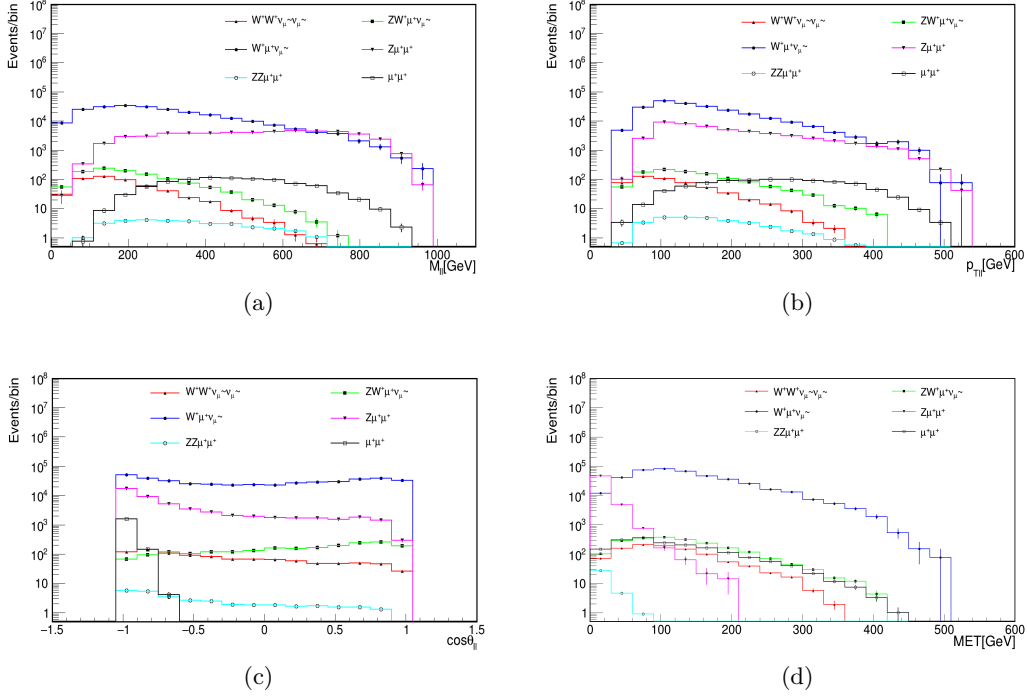
Figure 2: Simulation results of pure-leptonic channel, $\sqrt{s} = 1\text{TeV}, \mathcal{L} = 1 \text{ ab}^{-1}$. (a) invariant mass $M_{\ell\ell}$ distribution, (b) transverse momentum of leading lepton $p_{\text{T},\ell\ell}$ distribution, (c) $\cos\theta_{\ell\ell}$ ($\theta_{\ell\ell}$ is the angle between two leptons in final states) distribution, and (d) missing transverse energy $\not{E}_T$ distribution.

in final states. Among all variables, the $cos\theta_{\ell\ell}$ shows the most distinguishable behavior between the signals and backgrounds. The cut conditions in the pure-leptonic channel are listed in Table 1. The significance is defined as: $S = s/\sqrt{b} = 1.96$ (CL=95%), where s and b represent the number of signal and background events after all cuts, respectively. Since significance S is proportion to $|V_{\ell N_\alpha}|^4$, we can obtain the limit lines for the Majorana neutrinos masses range from 100GeV to 10TeV.

Table 1: The cut-flow table in the pure-leptonic channel.

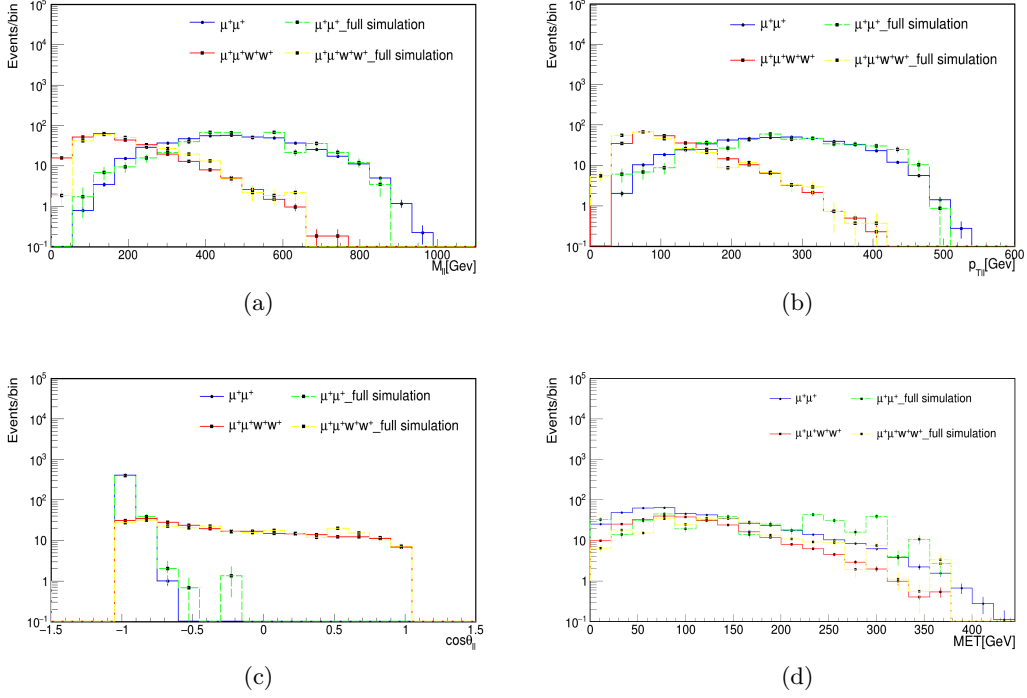| variables	limits
$M_{\ell\ell}$	$> 100.0\text{GeV}$
$p_{\text{T},\ell\ell}$	$> 120.0\text{GeV}$
$\not{E}_T$	$> 100.0\text{GeV}$
$cos\theta_{\ell\ell}$	< -0.95
$|\eta_\ell|$	< 2.5

Figure 3: Comparison of fast simulation and full simulation, $\sqrt{s} = 1\text{TeV}, \mathcal{L} = 1 \text{ ab}^{-1}$. (a) invariant mass $M_{\ell\ell}$ distribution, (b) transverse momentum of leading lepton $p_{\text{T},\ell\ell}$ distribution, (c) $\cos\theta_{\ell\ell}$ ($\theta_{\ell\ell}$ is the angle between two leptons in final states) distribution, and (d) missing transverse energy $\not{E}_T$ distribution.

4.2 Semi-leptonic channel

The constraints on the channel $\mu^+\mu^+ \to W^+W^+ \to \ell^+ 2j + \not{E}_T$ at $\sqrt{s} = 1\text{TeV}$ are: events must include exactly one lepton and two jets with $p_{\text{T}} > 20\text{GeV}$, $|\eta_\ell| < 2.5$, $|\eta_j| < 4.7$, and $\Delta R_{\ell j} > 0.4, \Delta R_{jj} > 0.4$. Fig. 4 shows the simulated distribution of reconstructed boson mass M_{jj} and the missing transverse energy $\not{E}_T$ in the semi-leptonic process. The $\not{E}_T$ distributions of the signal and all backgrounds are similar, so this variable can not be used to distinguish the signal from backgrounds. W boson can be reconstructed through M_{jj} in this channel, the signal and backgrounds shows more significant difference in M_{jj} distributions. The cuts applied in semi-leptonic channel are listed in Table 2. The simulation results show that semi-leptonic is the least sensitive channel.

4.3 Hadronic resolved channel

The constraints on channel $\mu^+\mu^+ \to W^+W^+ \to 4j$ at $\sqrt{s} = 1\text{TeV}$ are: events must include exactly four jets or two fatjets with $p_{\text{T}} > 20\text{GeV}$, $|\eta_j| < 4.7$, and $\Delta R_{jj} > 0.4$. The four jets are classified and clustered into two reconstructed "bosons" (W_1, W_2), their masses are denoted as M_1, M_2. We use the following algorithm:

- Construct all possible jet pairs candidates: (j_1j_2, j_3j_4), (j_1j_3, j_2j_4), and (j_1j_4, j_2j_3),
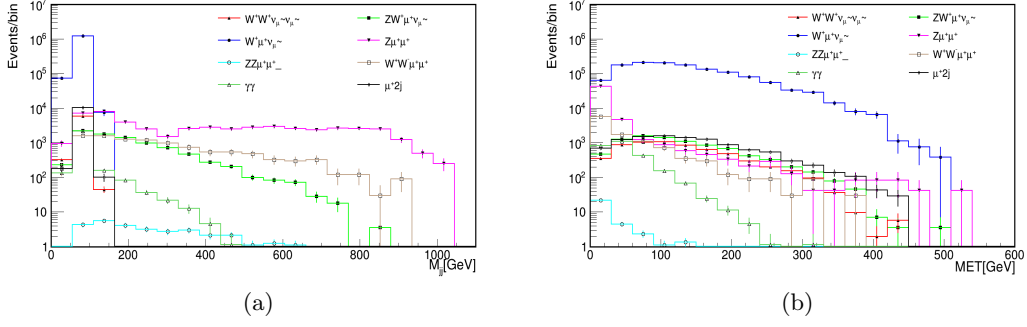
Figure 4: Semi-leptonic channel, $\sqrt{s} = 1\text{TeV}$, L=1 ab^{-1}. (a) the reconstructed W boson mass M_{jj} distribution, and (b) $\not{E}_T$ distribution.

Table 2: The cut-flow table in the semi-leptonic channel.

Variables	limits
M_{jj}	$< 140.0\text{GeV}$
$p_{\text{T},jj}$	$> 50.0\text{GeV}$
$p_{\text{T},\ell}$	$> 50.0\text{GeV}$
$\lvert\eta_j\rvert$	< 4.7
$\lvert\eta_\ell\rvert$	< 2.5

- Calculate the corresponding mass difference:

$$\Delta M^2 = (M_1 - M_W)^2 + (M_2 - M_W)^2, \tag{4.1}$$

- Choose the minimum ΔM^2 as the targeted jet pairs.

After the determination of the preferred combination of the jet pairs, we compare the signals with backgrounds using the variables related to the two final reconstructed W$^+$ boson candidates to find criteria for further optimization. Fig. 5 shows the distributions of several selected variables: four jets invariant mass M_{4j}, the transverse momentum of one reconstructed boson, $p_{\text{T},jj}$ and its mass, M_{jj}. The distributions show that M_{4j} is the most important variable to distinguish between the signals and backgrounds, and there's significant discrepancy between the signals and backgrounds are also shown in the distributions of the other two variables. The summary of cuts in hadronic processes is given in Table 3. The simulation results show that this channel is the most sensitive among the three channels at the same collision energy and luminosity.

For the implementation of the Boosted Decision Tree (BDT) method, we shuffle the signal and background events in hadronic state, and define the training and test sets with the event ratio of 1:1. We apply the per-event weight $n_{\mathcal{L}X} = \sigma_x \mathcal{L}/N_{GX}$ during the training to account for the cross-section difference among the processes, where σ_x is the cross-section of one process, $\mathcal{L}$ is the default target luminosity in this study (1 ab^{-1}) for a 1TeV muon collider, and N_{GX} is the total generated number of events [25]. We use variables
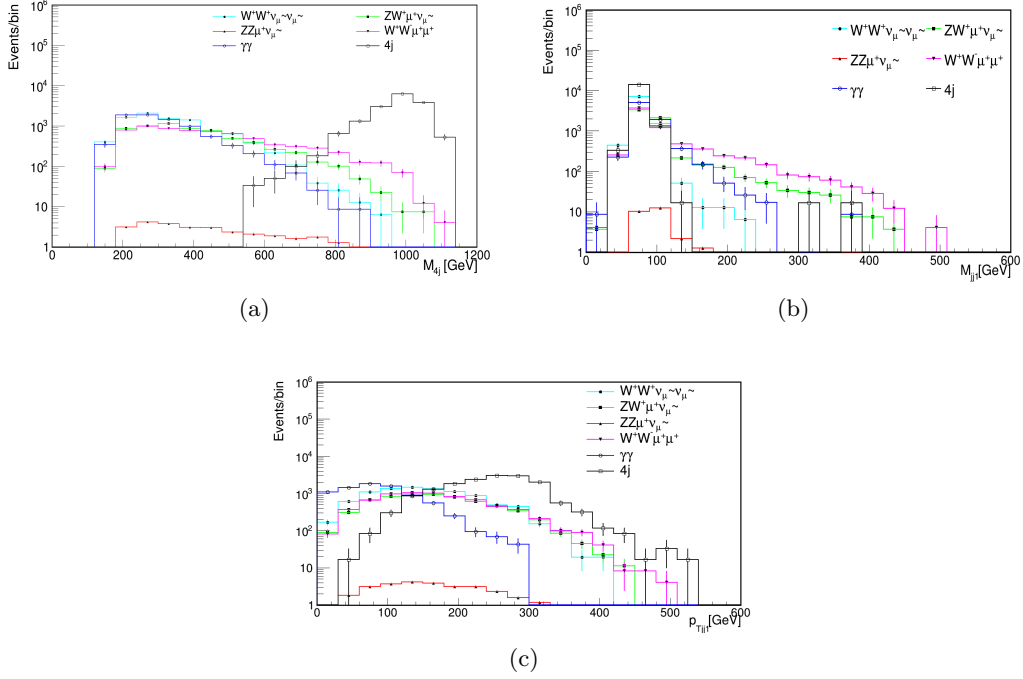
Figure 5: Simulation results of hadronic channel, $\sqrt{s} = 1\text{TeV}$, $\mathcal{L} = 1 \text{ ab}^{-1}$. (a) M_{4j} distribution, (b) M_{jj1} distribution, and (c) $p_{\text{T},jj1}$ distribution.

Table 3: The cut-flow table in the hadronic channel.

Variables	limits
M_{4j}	$> 600.0\text{GeV}$
$p_{\text{T},j_{1,2,3,4}}$	$> 50.0\text{GeV}$
$p_{\text{T},jj1}$	$[20\text{GeV}, 400\text{GeV}]$
$p_{\text{T},jj2}$	$[50\text{GeV}, 420\text{GeV}]$
M_{jj1}	$[50\text{GeV}, 110\text{GeV}]$
M_{jj2}	$[10\text{GeV}, 110\text{GeV}]$
$|\eta_j|$	< 4.7

$M_{4j}, M_{jj1}, p_{\text{T},jj1}, M_{jj2}, p_{\text{T},jj2}$ as input features, namely reconstructed kinematics of each event are used for training.

Fig. 6 shows the results of BDT. We provide p-values from the Kolmogorov-Smirnov test and the BDT score distributions for the signal and background in the training and test sets, as proof of no over-training in the BDT model. The receiver operating characteristic (ROC) curve of the trained model is then studied from the test sample, we find the background rejection is equal to 1, because the signal can be separated from the background completely when BDT score > 0.
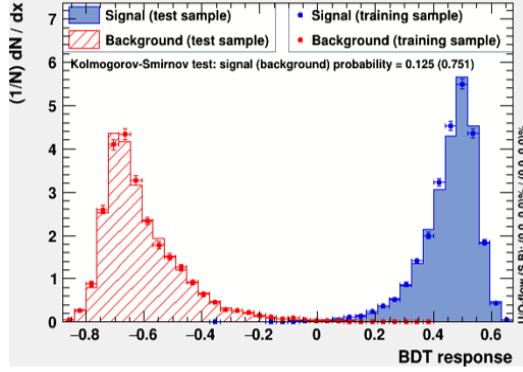
Figure 6: BDT training results in the hadronic channel at a $\sqrt{s} = 1\text{TeV}$ muon collider. The Kolmogorov-Smirnov test results and score distributions for signal and background in the training and test are presented.

4.4 Hadronic merged channel

When collision energy is several TeV, we must consider the boost effect when the two quarks from W^+ decay merged into a single fatjet with a mass around M_{W}. We use the processes at c.m. energy $\sqrt{s} = 10\text{TeV}$ to research this scenario. Fig. 7 shows some variables distribution of fatjet: the variables "Energy" and "E_t" are selected from SoftDroppedJet algorithm of fatjet, the variable τ_{N} is named N-subjettiness, which is a parameter to veto additional jet emissions and define an exclusive jet cross-section. It can be calculated through the equation:

$$\tau_N = \frac{1}{d_0} \sum_k p_{\text{T},k} \min \{\Delta R_{1,k}, \Delta R_{2,k}, \Delta R_{N,k}\}, \; d_0 = \sum_k P_{T,k} R_0. \tag{4.2}$$

The k runs over all constituent particles in a given jet, $p_{\text{T},k}$ is the transverse momentum of one particle, $\Delta R_{J,k}$ is the distance in the rapidity-azimuth plane between a candidate subjet J and a constituent particle k. d_0 is the normalization factor, R_0 is the characteristic jet radius used in the original jet clustering algorithm. N-subjettiness can be used to effectively "count" the number of subjets in a given jets [37]. In our analysis, we use τ_2/τ_1, which is a variable which can identify two-prong objects like boosted W boson, Z boson, and Higgs boson effectively. Table 4 gives the summary of cuts in this channel.

Table 4: The cut-flow table in the hadronic channel, with $\sqrt{s} = 10\text{TeV}$.

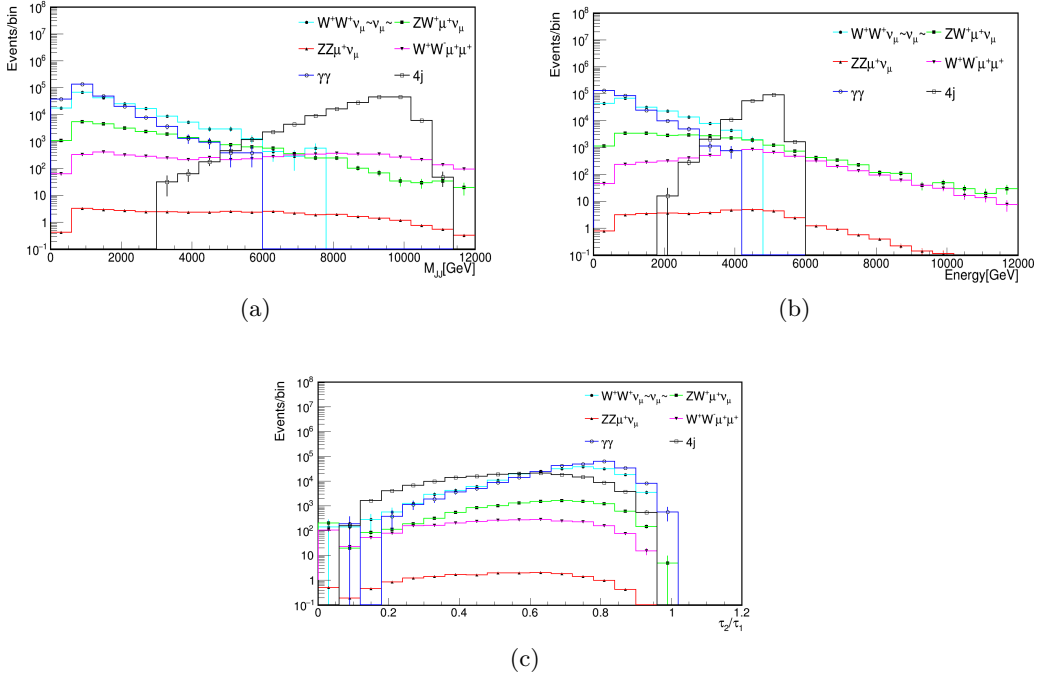| Variables	limits
Energy	$[2000.0\text{GeV}, 6000.0\text{GeV}]$
E_t	$[100\text{GeV}, 6000\text{GeV}]$
p_{T}	$[100\text{GeV}, 6000\text{GeV}]$
τ_2/τ_1	$[0.05, 0.95]$
M_{JJ}	$[3000\text{GeV}, 11000\text{GeV}]$
$|\eta_{FatJet}|$	< 5.0

Figure 7: Simulation results of hadronic channel, $\sqrt{s} = 10\text{TeV}, \mathcal{L} = 1 \text{ ab}^{-1}$. (a) the invariant mass of two fatjets, M_{JJ} distribution, (b) the energy distribution of fatjet in SoftDropped algorithm, and (c) τ_2/τ_1 distribution.

5   Results and Discussions

After analyzing four processes in three final states channels, we can obtain the exclusion limit of $|V_{\mu N_1}|$ of our signal channel: $\mu^+\mu^+ \to W^+W^+$. In Fig. 8, we present our simulation results of limit lines, as well as results from other experiments and simulations. The red solid line corresponds to the pure-leptonic processes at a muon collider($\mu^+\mu^+$) with $\sqrt{s} = 1\text{TeV}, \mathcal{L} = 1 \text{ ab}^{-1}$. The dark-blue line corresponds to the hadronic processes at a muon collider with $\sqrt{s} = 1\text{TeV}, \mathcal{L} = 1 \text{ ab}^{-1}$. The black line corresponds to the hadronic processes at a muon collider with $\sqrt{s} = 10\text{TeV}, \mathcal{L} = 1 \text{ ab}^{-1}$. The black dotted line corresponds to the hadronic processes at a muon collider with $\sqrt{s} = 10\text{TeV}, \mathcal{L} = 10 \text{ ab}^{-1}$. The solid brown and light-pink lines correspond to limits from considerations of viable leptogenesis scenarios [32]. The grey area is the region excluded by a global scan [33]. The yellow line corresponds to the experimental limits from prompt trilepton searches at the LHC [34]. The pink line shows the simulated limits from a future FCC-hh [35]. Three lines denoted ILC are simulated exclusion limits in future e^+e^- linear colliders [36]. Two groups of simulated results in $\mu^+\mu^-$ collider are also added [14, 15]. Our research gives simulated results for Majorana neutrinos masses range from 100 GeV to 40 TeV, it shows that better limitation is expected in the massive mass region ($M_N > 10\text{TeV}$), especially with hadronic processes at $\sqrt{s} = 10\text{TeV}$.
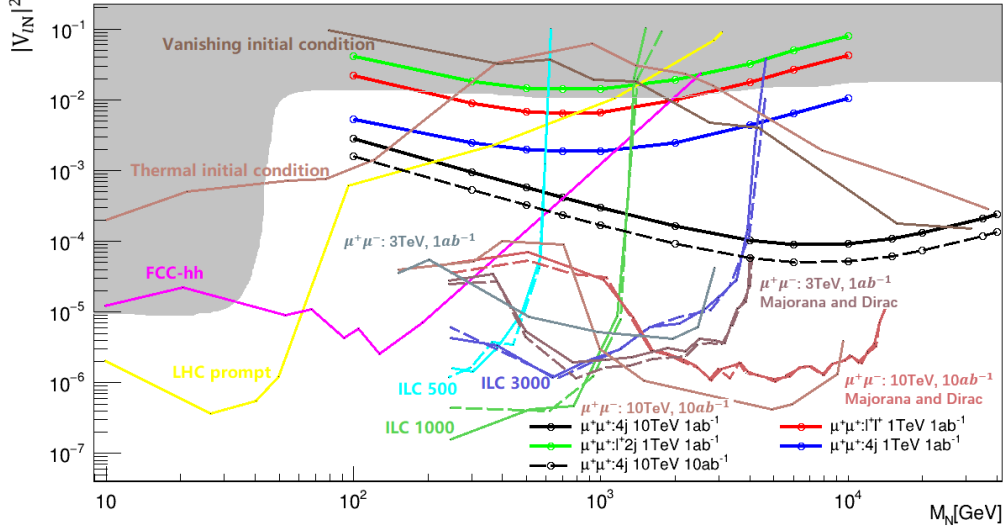
Figure 8: 2σ exclusion limit of $|V_{\mu N_1}|^2$ as a function of varying Majorana neutrino mass M_N. The green solid line corresponds to the semi-leptonic processes at a muon collider with $\sqrt{s} = 1$TeV, $\mathcal{L} = 1$ ab^{-1}. The red solid line corresponds to the pure-leptonic processes at a muon collider with $\sqrt{s} = 1$TeV, $\mathcal{L} = 1$ ab^{-1}. The dark-blue line corresponds to the hadronic processes at a muon collider with $\sqrt{s} = 1$TeV, $\mathcal{L} = 1$ ab^{-1}. The black line corresponds to the hadronic processes at a muon collider with $\sqrt{s} = 10$TeV, $\mathcal{L} = 1$ ab^{-1}. The black dotted line corresponds to the hadronic processes at a muon collider with $\sqrt{s} = 10$TeV, $\mathcal{L} = 10$ ab^{-1}. The experimental result from LHC and other simulation results are also added for comparison.

6 Conclusions and Outlook

In this paper, we investigate the potential of searching for Majorana neutrinos at future muon collider through the $\mu^+\mu^+ \to W^+W^+$ scattering process. It is a typical $0\nu\beta\beta$ like process and can be used to research LNV phenomenon. In our simulation, we focus on the collider phenomenology of $\mu^+\mu^+ \to W^+W^+$ process, to find the kinematic features that help to increase the detection potential, such as the distribution of $\cos\theta_{\ell\ell}$ in pure-leptonic processes and M_{4j} in hadronic processes. We have studied three final states and four different conditions with fast simulation, determined the value of mixing elements squared $|V_{\mu N_1}|^2$ corresponding to various Majorana neutrino mass at CL=95%. We also performed full simulation in pure-leptonic channel, the results show roughly similar distributions as fast simulation. Furthermore, we use BDT training on hadronic processes at $\sqrt{s} = 1$TeV, the result shows that the variable M_{4j} can be used to distinguish signal and backgrounds effectively. The distribution of some significant variables and associated cut-flow tables in pure-leptonic, semi-leptonic and hadronic channels are presented with collision energy $\sqrt{s} = 1$TeV and $\mathcal{L} = 1$ ab^{-1}. We studied the fatjet signature at collision energy $\sqrt{s} = 10$TeV, $\mathcal{L} = 1$ ab^{-1} and 10 ab^{-1} respectively, it turns out that these channels provide

the strongest limitation. Compared with other researches as shown in Fig. 8, our analysis shows a unique advantage of using the same sign muon collider in searching of Majorana neutrinos, especially in the mass region above 10TeV.

Acknowledgments

References

[1] S. Chatrchyan et al. [CMS Collaboration], Phys. Lett. B **716**, 30 (2012) [arXiv:1207.7235 [hep-ex]].

[2] G. Aad et al. [ATLAS Collaboration], Phys. Lett. B **716**, 1 (2012) [arXiv:1207.7214 [hep-ex]].

[3] A. M. Sirunyan *et al.* [CMS], Phys. Rev. Lett. **120**, no.22, 221801 (2018) doi:10.1103/PhysRevLett.120.221801 [arXiv:1802.02965 [hep-ex]].

[4] G. Aad *et al.* [ATLAS], JHEP **10**, 265 (2019) doi:10.1007/JHEP10(2019)265 [arXiv:1905.09787 [hep-ex]].

[5] A. M. Sirunyan *et al.* [CMS], JHEP **03**, 051 (2020) doi:10.1007/JHEP03(2020)051 [arXiv:1911.04968 [hep-ex]].

[6] A. M. Sirunyan *et al.* [CMS], JHEP **01**, 122 (2019) doi:10.1007/JHEP01(2019)122 [arXiv:1806.10905 [hep-ex]].

[7] M. Aaboud *et al.* [ATLAS], JHEP **01**, 016 (2019) doi:10.1007/JHEP01(2019)016 [arXiv:1809.11105 [hep-ex]].

[8] [CMS], [arXiv:2206.08956 [hep-ex]].

[9] P. Abreu *et al.* [DELPHI], Z. Phys. C **74**, 57-71 (1997) [erratum: Z. Phys. C **75**, 580 (1997)] doi:10.1007/s002880050370

[10] F. M. L. Almeida, Jr., Y. do Amaral Coutinho, J. A. Martins Simoes and M. A. B. do Vale, Eur. Phys. J. C **22**, 277-281 (2001) doi:10.1007/s100520100798 [arXiv:hep-ph/0101077 [hep-ph]].

[11] Y. Zhang and B. Zhang, JHEP **02**, 175 (2019) doi:10.1007/JHEP02(2019)175 [arXiv:1805.09520 [hep-ph]].

[12] K. Wang, T. Xu and L. Zhang, Phys. Rev. D **95**, no.7, 075021 (2017) doi:10.1103/PhysRevD.95.075021 [arXiv:1610.02618 [hep-ph]].

[13] H. Gu and K. Wang, Phys. Rev. D **106**, no.1, 015006 (2022) doi:10.1103/PhysRevD.106.015006 [arXiv:2201.12997 [hep-ph]].

[14] T. H. Kwok, L. Li, T. Liu and A. Rock, [arXiv:2301.05177 [hep-ph]].

[15] P. Li, Z. Liu and K. F. Lyu, [arXiv:2301.07117 [hep-ph]].

[16] J. L. Yang, C. H. Chang and T. F. Feng, [arXiv:2302.13247 [hep-ph]].

[17] A. M. Sirunyan *et al.* [CMS], Phys. Lett. B **812**, 136018 (2021) doi:10.1016/j.physletb.2020.136018 [arXiv:2009.09429 [hep-ex]].

[18] Daniel Schulte, Nadia Pastrone, Ken Long, CERN Cour. 60 (2020) 3, 41-46.

[19] Mario Greco, Tao Han, Zhen Liu, Physics Letters B **763** (2016) 409-415.

[20] Dario Buttazzo, et al., J. High Energ. Phys. **11**, 144 (2018).

[21] Hind Al Ali, et al., arXiv:2103.14043.

[22] Mauro Chiesa, et al., arXiv:2003.13628.

[23] Nazar Bartosik, et al., arXiv:2001.04431.

[24] J. Alwall, R. Frederix, S. Frixione, V. Hirschi, F. Maltoni, O. Mattelaer, H. S. Shao, T. Stelzer, P. Torrielli and M. Zaro, JHEP **07**, 079 (2014) doi:10.1007/JHEP07(2014)079 [arXiv:1405.0301 [hep-ph]].

[25] T. Yang, S. Qian, Z. Guan, C. Li, F. Meng, J. Xiao, M. Lu and Q. Li, Phys. Rev. D **104**, no.9, 093003 (2021) doi:10.1103/PhysRevD.104.093003 [arXiv:2107.13581 [hep-ph]].

[26] D. Buarque Franzosi, O. Mattelaer, R. Ruiz and S. Shil, JHEP **04**, 082 (2020) doi:10.1007/JHEP04(2020)082 [arXiv:1912.01725 [hep-ph]].

[27] T. Sjöstrand, S. Ask, J. R. Christiansen, R. Corke, N. Desai, P. Ilten, S. Mrenna, S. Prestel, C. O. Rasmussen and P. Z. Skands, Comput. Phys. Commun. **191**, 159-177 (2015) doi:10.1016/j.cpc.2015.01.024 [arXiv:1410.3012 [hep-ph]].

[28] M. Cacciari, G. P. Salam and G. Soyez, Eur. Phys. J. C **72**, 1896 (2012) doi:10.1140/epjc/s10052-012-1896-2 [arXiv:1111.6097 [hep-ph]].

[29] M. Cacciari, G. P. Salam and G. Soyez, JHEP **04**, 063 (2008) doi:10.1088/1126-6708/2008/04/063 [arXiv:0802.1189 [hep-ph]].

[30] J. de Favereau *et al.* [DELPHES 3], JHEP **02**, 057 (2014) doi:10.1007/JHEP02(2014)057 [arXiv:1307.6346 [hep-ex]].

[31] F. F. Deppisch, P. S. Bhupal Dev and A. Pilaftsis, New J. Phys. **17**, no.7, 075019 (2015) doi:10.1088/1367-2630/17/7/075019 [arXiv:1502.06541 [hep-ph]].

[32] M. Drewes, Y. Georis and J. Klarić, Phys. Rev. Lett. **128**, no.5, 051801 (2022) doi:10.1103/PhysRevLett.128.051801 [arXiv:2106.16226 [hep-ph]].

[33] M. Chrzaszcz, M. Drewes, T. E. Gonzalo, J. Harz, S. Krishnamurthy and C. Weniger, Eur. Phys. J. C **80**, no.6, 569 (2020) doi:10.1140/epjc/s10052-020-8073-9 [arXiv:1908.02302 [hep-ph]].

[34] E. Izaguirre and B. Shuve, Phys. Rev. D **91**, no.9, 093010 (2015) doi:10.1103/PhysRevD.91.093010 [arXiv:1504.02470 [hep-ph]].

[35] S. Antusch, E. Cazzato and O. Fischer, Int. J. Mod. Phys. A **32**, no.14, 1750078 (2017) doi:10.1142/S0217751X17500786 [arXiv:1612.02728 [hep-ph]].

[36] K. Mekała, J. Reuter and A. F. Żarnecki, JHEP **06**, 010 (2022) doi:10.1007/JHEP06(2022)010 [arXiv:2202.06703 [hep-ph]].

[37] J. Thaler and K. Van Tilburg, JHEP **03**, 015 (2011) doi:10.1007/JHEP03(2011)015 [arXiv:1011.2268 [hep-ph]].

[38] https://ilcsoft.desy.de/portal.

[39] N. Bartosik *et al.* [Muon Collider], [arXiv:2203.07964 [hep-ex]].

[40] A. Buckley, J. Butterworth, S. Gieseke, D. Grellscheid, S. Hoche, H. Hoeth, F. Krauss, L. Lonnblad, E. Nurse and P. Richardson, *et al.* Phys. Rept. **504**, 145-233 (2011) doi:10.1016/j.physrep.2011.03.005 [arXiv:1101.2599 [hep-ph]].

[41] https://github.com/iLCSoft/Marlin

[42] https://github.com/delphes/delphes/blob/master/cards/delphes_card_MuonColliderDet.tcl